REPORT DOCUMENTATION PAGE

Form Approved
OMB No. 0704-0188

1. REPORT DATE *(DD-MM-YYYY)*	**2. REPORT TYPE**	**3. DATES COVERED** *(From - To)*
December 2013	Technical Paper	December 2013- July 2014

4. TITLE AND SUBTITLE
MODELING OF FUEL FILM COOLING ON CHAMBER HOT WALL

5a. CONTRACT NUMBER
In-house

5b. GRANT NUMBER

5c. PROGRAM ELEMENT NUMBER

6. AUTHOR(S)
A. Himansu, E.B. Coy, V. Sankaran

5d. PROJECT NUMBER

5e. TASK NUMBER

5f. WORK UNIT NUMBER
Q0VZ

7. PERFORMING ORGANIZATION NAME(S) AND ADDRESS(ES)

Air Force Research Laboratory (AFMC)
AFRL/RQRC
10 E. Saturn Blvd.
Edwards AFB, CA, 93524-7680

8. PERFORMING ORGANIZATION REPORT NO.

9. SPONSORING / MONITORING AGENCY NAME(S) AND ADDRESS(ES)

Air Force Research Laboratory (AFMC)
AFRL/RQR
5 Pollux Drive.
Edwards AFB, CA, 93524-7048

10. SPONSOR/MONITOR'S ACRONYM(S)

11. SPONSOR/MONITOR'S REPORT NUMBER(S)
AFRL-RQ-ED-TP-2013-285

12. DISTRIBUTION / AVAILABILITY STATEMENT
Approved for public release; distribution unlimited

13. SUPPLEMENTARY NOTES
Technical Paper presented at 50th AIAA/ASME/SAE/ASEE Joint Propulsion Conference; Cleveland, Ohio, 28 - 30 July 2014. PA# 14068

14. ABSTRACT

A numerical model is constructed to simulate hydrocarbon fuel film cooling of the hot-gas side of liquid rocket engine chamber walls. The model consists of the steady Reynolds-averaged Navier-Stokes equations for multi-species flow with heat transfer and equilibrium chemistry. Preliminary results are presented in this extended abstract. The predictive performance of the model is studied by comparison to experimental heat flux data. Several flow conditions and film cooling mass flow rates were used in the simulation case matrix. Comparisons between numerical predictions of the wall surface heat flux and experimental data are used to guide further development of the model which is expected to provide improved predictions in the final version of the paper. Good agreement was obtained in one case with no film cooling, if radiative heat transfer was included in the model. A key finding is that radiative heat flux is comparable to convective heat flux upstream of the injection slot, as shown by the current numerical simulations. Several physics and chemistry aspects are identified that are not properly accounted for in the current model. The chief of these is soot formation and the deposit of a thermal barrier coating of carbon on the wall. Most of these aspects are currently being addressed to improve the model, and results using a model with improved accuracy will be reported in the final paper.

15. SUBJECT TERMS

16. SECURITY CLASSIFICATION OF:			**17. LIMITATION OF ABSTRACT**	**18. NUMBER OF PAGES**	**19a. NAME OF RESPONSIBLE PERSON**
					Ed Coy
a. REPORT	**b. ABSTRACT**	**c. THIS PAGE**	SAR	25	**19b. TELEPHONE NO** *(include area code)*
Unclassified	**Unclassified**	**Unclassified**			661-275-5219

Standard Form 298 (Rev. 8-98)
Prescribed by ANSI Std. 239.18

[1]MODELING OF FUEL FILM COOLING ON CHAMBER HOT WALL

A. Himansu, E.B. Coy, V. Sankaran, S.A. Danczyk
Air Force Research Laboratory
Edwards AFB, CA

ABSTRACT

A numerical model is constructed to simulate hydrocarbon fuel film cooling of the hot-gas side of liquid rocket engine chamber walls. The model consists of the steady Reynolds-averaged Navier-Stokes equations for multi-species flow with heat transfer and equilibrium chemistry. Preliminary results are presented in this extended abstract. The predictive performance of the model is studied by comparison to experimental heat flux data. Several flow conditions and film cooling mass flow rates were used in the simulation case matrix. Comparisons between numerical predictions of the wall surface heat flux and experimental data are used to guide further development of the model which is expected to provide improved predictions in the final version of the paper. Good agreement was obtained in one case with no film cooling, if radiative heat transfer was included in the model. A key finding is that radiative heat flux is comparable to convective heat flux upstream of the injection slot, as shown by the current numerical simulations. Several physics and chemistry aspects are identified that are not properly accounted for in the current model. The chief of these is soot formation and the deposit of a thermal barrier coating of carbon on the wall. Most of these aspects are currently being addressed to improve the model, and results using a model with improved accuracy will be reported in the final paper.

INTRODUCTION

The walls of liquid rocket engine chambers and nozzles must contain large pressures while being exposed to very high temperature gases, and therefore must be cooled to maintain their structural integrity. The two chief technologies to keep the walls cool are (a) rapid heat removal by passing cool fuel through numerous channels embedded in the walls, and (b) shielding of the wall from hot gases by injection of a cool fuel or oxidizer film onto the wall. In the pursuit of higher power density, rocket engine designers are now considering greater propellant mass fluxes than in previous designs. This results in higher heat fluxes to engine walls, such that the walls cannot be sufficiently cooled by embedded regenerative fuel coolant technology alone, making film cooling essential. The high reactivity of the oxidizer with the metal walls usually means that fuel must be used as the film coolant. The current study is the first phase in a hydrocarbon fuel film cooling (FFC) simulation and design optimization project.

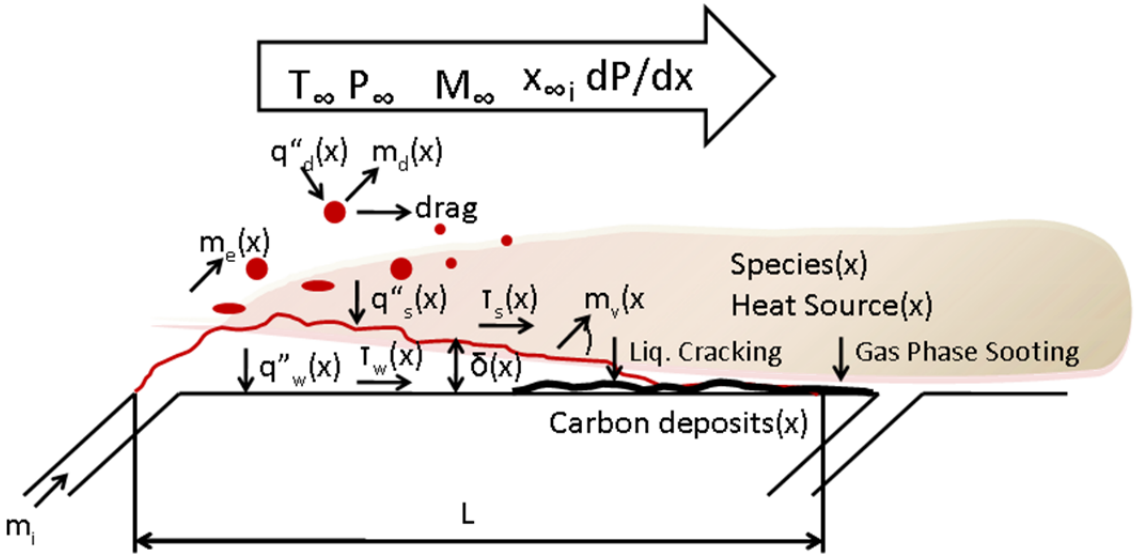

Figure 1. Film cooling with a liquid hydrocarbon fuel

We describe now the physical and chemical phenomena involved in hydrocarbon FFC. Figure 1 is a notional diagram of the processes involved. Hydrocarbon fuel at fuel tank temperature is injected through a slot into a high-speed high-temperature turbulent reacting cross flow at supercritical pressure. The fuel jet and the cross-flow interact. Some part of the jet is stripped off and entrained by the hot gas. This portion disperses and mixes with the high-speed hot gas away from the wall, and does not contribute very much to cooling the wall. The rest of the jet is forced by momentum exchange to form a film on the wall, which serves to keep the wall cooler than in the absence of the film. The film is kept in motion along the wall by shear forces exerted by the hot gas. As hot gas and film travel downstream at different speeds, there is a mutual exchange of mass, momentum and energy. As the fluid in the film heats up, it undergoes cracking or pyrolysis, and some of the resultant species undergo oxidation by the excess oxidizer diffusing from the hot cross flow. The pyrolysis produces a further cooling effect by its endothermic nature. When the products of pyrolysis diffuse into the hot gas, soot formation often occurs, followed by some soot destruction by oxidation. Some of the soot is transported to the wall by turbulent mass diffusion. There, surface chemistry and physics come into play, and carbonaceous deposits are formed on the wall. This carbon layer can provide substantial wall protection by acting as a thermal barrier. Further downstream, when the film has been depleted of its cooling and coking capacities, a second slot is needed to inject fresh cool fuel. All of these processes pose great challenges to modelers. The supercritical pressure makes information on equation of state and transport properties hard to come by. The large temperature range causes large variations in fluid properties, reaction rates and composition. The detailed chemistry of hydrocarbon combustion, pyrolysis, soot formation, and soot oxidation can involve hundreds of species and thousands of reactions. The transport of soot particulates, and the surface physics and chemistry of wall deposition, and change of effective wall thermal resistance are all very complex to simulate numerically. Furthermore, radiative heat transfer through an absorbing-emitting medium, and conjugate heat transfer coupling the convective heat transfer in the fluid with the heat conduction occurring in the metal wall further complicate the modeler's task.

There is vast literature on the modeling and simulation of film cooling for gas turbine engines. In that area, the film is used to cool the turbine stator blades downstream of the combustor. The models do not usually involve chemical reactions, as the film fluid is air bled from the high-pressure compressor. The temperatures and pressures encountered are also not as extreme as those found in liquid rocket engines. There is also some literature on hydrogen film cooling modeling. There is scant literature on the modeling of hydrocarbon fuel film cooling at supercritical pressures. A relevant recent simulation study by Yang and Sun [1] used a finite-rate laminar chemistry approach, including the T.S. Wang kerosene combustion mechanism [7], to

model kerosene film cooling and the attendant pyrolysis reactions. Their study did not attempt to validate the simulations with experimental data. Kirchberger, Schlieben and Haidn [2] used analytical and semi-empirical formulas to predict the cooling effect of films, and obtained comparison with experiment that they deemed unsatisfactory.

The current study is the first modeling and simulation (M&S) phase of a project to advance hydrocarbon FFC technology for liquid rocket engines. The goals of the M&S effort are to provide validated predictive physics-based numerical simulation tools for design optimization of FFC. Design optimization would involve tailoring the FFC injection slot spacing and the FFC mass and momentum fluxes to provide adequate wall protection while minimizing the loss of specific impulse due to partial and non-optimal fuel combustion. The approach taken in the M&S effort is to construct a model of the FFC physics and chemistry using available M&S tools. We then evaluate the strengths and weaknesses of the model by numerically solving it and validating the results against lab-scale experimental data. We will address most of the model shortcomings identified through the preliminary results shown here, and provide an improved model and improved predictions in the final paper.

EXPERIMENTAL CASES AND SELECTED VALIDATION CASES

In the preliminary results shown in this abstract, numerical simulations were performed for cases corresponding to experiments performed in our laboratory. A nominal chamber pressure of 700 psi was used for all cases. The mixture ratio was 2.8. Two different core mass flow rates (CMFR) were used, referred to as “large” and “small”. With the large CMFR, in addition to a non-film-cooled case, cases corresponding to FFC mass flow rates of 0.6%, 1.5% and 2.9% of the CMFR were run. With the small CMFR, a non-FFC case as well as cases with FFC mass flow rates of 1.5%, 3% and 6% of the CMFR were run. Since all FFC cases involve very high ratios of the core flow momentum flux to the FFC momentum flux, the values of FFC mass flow rate as a percentage of the CMFR are of significance, while the absolute values are not. The heat flux values for both experiments and simulations are also normalized, in order to assess the relative performance of the FFC. A simulation was also performed that included radiative heat transfer using the P1 radiation model.

The gas flow-path from the injector face to the to the test section includes an acoustic cavity section, an igniter section, a straight section square cross-section, a section that transitions to a straight section of a smaller square cross-section, which in turn leads to the test section. Downstream of the measurement panel are a square-to-round transition section and a nozzle exhausting to the atmosphere. The walls of the entire flow-path are water-cooled.

.

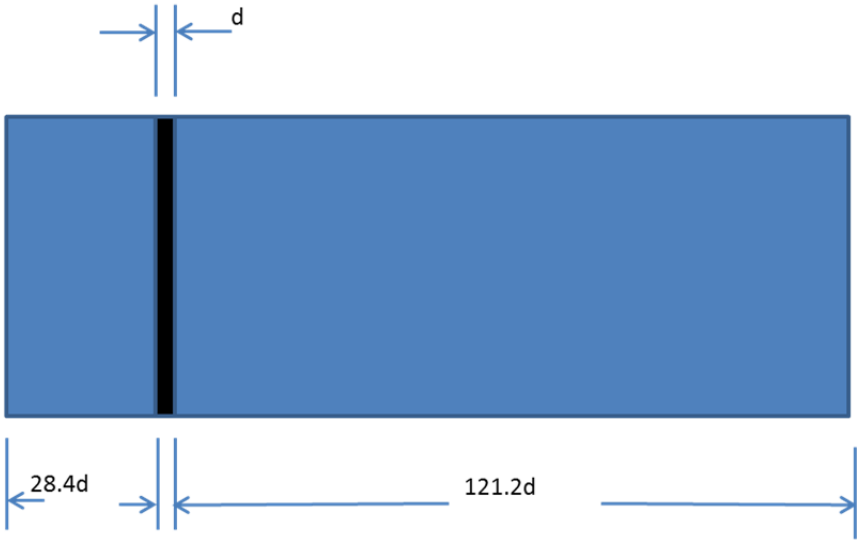

Figure 2. Schematic of FFC panel used in experiments of Coy and Danczyk

Figure 2 is a schematic view of the heat flux measurement panel of the test article used in the experiments, with the dimensions listed in terms of *d*, the slot "length" or streamwise extent. The slot is seen as a black stripe at about a fifth of the length from the left side of the figure. The figure shows the surface of the panel as viewed from within the test article. The panel forms one of the four walls of that section, hereafter called the test section, of the test article. The hot gases created by the primary combustion in the gas generator upstream of the test section flow over the panel from left to right in the figure. The portions of the panel both upstream and downstream of the slot house multiple water calorimeters, with water passages embedded beneath the panel surface and running parallel to the slot. Each calorimeter measures the panel surface heat flux averaged over its own exposed surface area. The calorimeters serve also to cool the wall and thereby preserve its structural integrity. RP-2 fuel was injected through the FFC slot from injection manifolds under the wall. The injected RP-2 provided film cooling of the exposed panel surface downstream of the slot.

NUMERICAL MODELS AND SIMPLIFYING APPROXIMATIONS

Not all of the physics and chemistry described in the Introduction is modeled in the present study. The approach we took here was to begin with the simplest plausible model incorporating the physics known to be important in FFC. Then we performed preliminary simulations reported in this extended abstract and evaluated the accuracy of the predictions for some validation cases. We used the information obtained in these preliminary simulations to suggest improvements in the model. The model is currently being refined and tested, and the resulting improved predictions will be reported in the final version of the paper to be presented at the conference. We describe here the modeling choices made and the model constructed, but we do not provide the mathematical representation of the model and its sub-models, because these are well-established and readily available in standard textbooks on CFD, chemical thermodynamics and transport phenomena.

Detailed experimental measurements of flow conditions in rocket engines are notoriously difficult to obtain, due to the extreme conditions of temperature and pressure. Furthermore, to produce controllable conditions in the laboratory that approach those in rocket engines, the experimental arrangement will necessarily involve scaled-down versions of many elements found in full-scale engines. It may be prohibitively expensive to perform multiple simulations of the entire experimental arrangement. Experiment and simulation must therefore co-evolve, with

computational model sensitivity studies helping to identify which model simplifications are allowable within accuracy goals, and where more detailed measurements in future experiments are needed to introduce appropriate computational boundaries.

First, we list and discuss the omissions and approximations we made in modeling both the fluid behavior and the constraints imposed in the experiments. Then we describe the resulting model. The omissions and simplifications are:

1. A Reynolds-averaged steady mean flow representation is used, and the effect of the fluid turbulence on the mean flow is approximated by including a Reynolds-averaged Navier-Stokes (RANS) turbulence model as part of the computational model. This approximation was made to reduce the computational cost of the simulation and data post-processing.
2. The flow from the injector face to the beginning of the test section is treated as a 'run-up' section relative to the test section, and is computed separately prior to the computation in the test section. The velocities, temperature and turbulence quantities at the outlet of the run-up are used as inlet boundary conditions for the computations in the test section. The run-up flow is computed for two flow conditions, corresponding to the two CMFR values considered. The detailed combustion process and flame downstream of the injector are not modeled in the run-up simulation. The entire process is instead represented by assuming the combustion to be complete at the injector face. The fluid at the inlet section of the run-up is taken to be in the fully combusted state predicted by a quasi-one-dimensional equilibrium chemistry calculation performed using the Chemical Equilibrium with Applications (CEA) computer program of [3]. This simplification is deemed acceptable for our purpose, because if the propellant mixing and combustion are effective, the state of the core fluid at entry to the test section should be homogeneous and very similar to that predicted by CEA. The thermal boundary condition at the walls of the run-up is not well-characterized in the experiment. We used a constant wall temperature of 800 K as a representative value. This will result in thermal state of the fluid at entry to the test section being somewhat different from that in the experiment, depending on how much heat was lost through the walls. In the final full version of this paper, we will remove the uncertainty inherent in this simplification by performing a conjugate heat transfer simulation that includes the effect of the water-cooling on the other side of the walls.
3. The flow in both run-up and test sections is assumed to be two-dimensional. This neglects the boundary-layer thickening at the edges formed by the corners of the square cross-section. It also neglects the boundary-layer thinning and core-flow non-uniformity caused by the area contraction of the cross-section. Post-experimental photographs of the soot layer deposited on the panels suggest some variation of the film thickness in the span-wise direction. However, in keeping with the two-dimensional modeling assumption, the details of the fuel film injection arrangements are neglected. The FFC injection manifold is modeled by a straight duct of constant cross-section, with walls at right-angles to the test panel wall.
4. The core flow and wall film in the test chamber are thermally strongly coupled through the highly conductive copper panel wall to the calorimeter system beneath the panel surface. To properly simulate the experiments, we would need to perform conjugate heat transfer simulations that include the conduction in the wall and the convection to the water channels in the calorimeters. The measured water temperatures at calorimeter inlets and outlets and the measured water mass flow rate would serve as the water boundary conditions. For the final version of the paper, these conjugate heat transfer simulations will be performed. For the preliminary results shown in this abstract, we introduced a computational boundary at the hot wall surface. Aside from the no-slip and no-injection conditions on the velocity, a thermal boundary condition is required at this boundary. We have a choice between specifying the wall surface heat-flux and specifying the wall surface temperature. Of the two quantities, the flow simulation would yield the quantity not specified. We elected to specify the wall temperature, because this would minimize the error in the assigned temperature-dependent molecular fluid properties. The latter have a significant effect on the predicted thermal behavior at the wall. In the

experiments, the calorimetry yielded surface heat-flux measurements. We chose to assume a constant wall temperature as a boundary condition in most of the simulations. A value of 800 K was selected as being representative. We reasoned that since the core gas temperature was around 3680 K, the assumed wall temperature would incur only a small fractional error in the driving temperature difference and thus in the predicted heat flux. However, this reasoning does not hold just downstream of the fuel injection, where the driving temperature difference is reduced because of the low temperature of the fuel.

5. The fluid in the chamber is taken to be a mixture of the hot gases and the fuel injected via the FFC slot. The mixture is assumed to obey an ideal gas equation of state. Kerosene vapor is used as a simulant for the injected fuel. The behavior of RP-2 or kerosene at room temperature and supercritical pressure is known to depart significantly from ideal gas behavior. For the results shown in this abstract, the transport properties of the mixture are taken to be constant and equal to those of the hot gas at 800 K, as predicted by CEA [3]. For the final version of the paper, more accurate modeling of the molecular transport properties will be used, to account for dependence on temperature pressure and mixture composition. The assumption that the fuel and hot gases are perfectly miscible fluid species also precludes the capturing of interfacial instabilities between core flow and film, and the subsequent fuel stripping, and dispersion. For the simulation involving radiative heat transfer, the radiation absorption coefficient was taken to be100 per meter. This lies somewhat on the high side of a range of expected wavelength-averaged values for typical gases, but may be reasonable for a sooty gas. The estimation of the mean absorption coefficient of gaseous mixtures, particularly if particulates such as soot are present, is a complex process, as seen in Chapter 10 of Modest [4], and was deferred to future work. For the final version of the paper, a better estimate of the absorption coefficient will be sought.
6. With regard to the chemical reactions taking place, several modeling approximations of varying levels of computational cost are possible. The biggest simplification, of course, would come from neglecting chemical effects altogether. This would result in the cheapest simulations, but would completely miss the endothermic effect of fuel pyrolysis that was discussed in the introductory section. The next step up with regard to computational cost, and the approach taken here, is to assume that the mixture is in chemical equilibrium at all stages of the mixing between core flow and film. This is equivalent to assuming that the chemical reactions caused by the mixing of fuel and hot combustion products that include oxygen are much faster than the fluid convection, and that they proceed to completion. Such an approximation allows the use of a conserved scalar approach to accounting for changes in chemical composition. This approach is computationally considerably cheaper than using finite-rate chemistry for the pyrolysis and oxidation. Well-validated finite-rate chemistry models for kerosene pyrolysis, oxidation and sooting are difficult to find in the literature, and are likely to be stiff systems of differential equations. This makes them very expensive to solve.
7. The sooting and wall coke deposition seen in the experiments are not modeled in the current phase of this project. As discussed in the introductory section, sooting and coking are notoriously complex topics. CFD with detailed chemistry and transport of soot would be computationally impractical for a model intended for use in design optimization. Well-validated global reduced kinetic mechanisms are needed to keep the computational cost within reason. In the current phase of this modeling effort, we have omitted accurate models for sooting. In the final paper, we will introduce the simplest model to represent the thermal effect of the carbon deposition: a constant thermal resistance downstream of the injection slot.
8. The computational domain was truncated to include only half the chamber in the vertical direction. This was done to save computational effort, which would be especially important in future simulations if finite-rate chemistry with stiff equations is considered. A symmetry boundary condition was imposed at the artificial boundary thus created. Because of the distance between upper and lower walls, this simplification should have relatively little effect on the interaction between the chamber core flow and the fuel film. However, it is equivalent to introducing a fuel injection slot on the upper wall and thus

doubling the amount of fuel injected. This results in the centerline velocity increasing twice as much from the no-injection case, as compared to the experimental reality.

Next, we discuss the model used in all the simulations. We assembled the model in the ANSYS Fluent 14 commercial CFD software. Fluent 14 was used for all simulations reported here. The model uses the two-dimensional, steady-state, compressible, pressure-based Reynolds-averaged Navier-Stokes (RANS) solver with heat transfer. The RANS turbulence model used is the Shear Stress Transport (SST) k-ω model in the solution-to-wall mode without the use of wall functions. As discussed previously, the fluid was modeled as a multi-species fluid with equilibrium chemistry. Fluid properties for the individual species present in the fluid mixture are available in the standard Fluent properties database. From the properties of the individual species, Fluent calculates thermodynamic properties of the mixture based on its composition and temperature. This leaves only the transport properties of the fluid mixture, namely the molecular (laminar) viscosity and the molecular thermal conductivity, as specifiable by the user when assembling the model. One of the simulations included a sub-model, the P1 radiation model, to account for radiative heat transfer. The fluid mixture was assumed to be a participating medium for radiation. In particular, it was assumed to be a gray medium, which refers to the assumption that the radiation absorption coefficient of the fluid is independent of the wavelength of the radiation.

In this paragraph and the next, we summarize for the reader the conserved scalar approach taken in the model to track changes in the equilibrium chemical composition and account for turbulence-chemistry interaction. Details of this approach may be found in Peters [5] and in more recent literature on the topic. To simulate flow of a pure substance, we must solve coupled partial differential equations (PDEs) representing balance of mass, momentum and enthalpy. In the conventional laminar finite-rate chemistry approach, if n chemical species are present in the multi-component fluid, $n-1$ additional PDEs for species conservation must be coupled with mass, momentum and enthalpy balances. If the number of species is large, this adds greatly to the cost of solving the system. These additional PDEs contain source terms representing rates of creation or destruction of species via chemical reactions. These source terms can render the system numerically stiff, and greatly increase the difficulty and cost of obtaining a stable solution.

In contrast to the above situation, in the conserved scalar approach used here, the $n-1$ PDEs for species conservation are replaced by just two PDEs, one for conservation of the mean mixture fraction, f, and another for conservation of the variance, f', of f. This is much less expensive than tracking n-1 species. Furthermore, there are no chemistry source terms in these conservation equations, and so the system is relatively well-conditioned. The mixture fraction at any time and spatial point is defined as the mass fraction of the fluid that originated in the fuel stream. Thus f serves to distinguish between a 'fuel' species and an 'oxidizer' species. The variance f' arises from a probability distribution function (PDF) representation of the turbulent fluctuations of the instantaneous mixture fraction. The mean values of density, temperature and individual species mass fractions must be calculated from values of f, f' and the mean enthalpy, h. Fluent pre-computes these relationships and stores them in a look-up table of PDFs that is used during the flow simulation, i.e. while numerically solving the conservation PDEs. In the current model, this is done by using equilibrium thermochemistry methods and knowledge of the specific heat as a function of temperature. In obtaining mean values from relationships that apply to instantaneous values, Fluent uses an assumed-shape PDF termed the β-Function PDF. This PDF is commonly used for this purpose in the literature, and it, with the particular shape parameters used in conjunction with it in Fluent, closely resemble experimentally observed PDFs (see Peters [5] for details). The conserved scalar formulation just described is a topic of active current research in the simulation of turbulence-chemistry interaction. However, for our purposes it is sufficient to note that it is ideal for non-premixed multi-component turbulent flow with equilibrium chemistry, where it is equivalent to a 'mixed is reacted' assumption. Furthermore, the formulation can be applied to reacting turbulent flows with moderately non-equilibrium chemistry via flamelet models. We may follow this path in future work.

To describe the spatial computational domain that was selected, we use two-dimensional rectangular Cartesian coordinates x and y, with the streamwise "length" of the slot, d, as the unit

of length. The film-cooled panel wall is located at y=0. The trailing edge of the FFC injection slot is located at x=0, i.e. at the origin. The domains for both the run-up and the panel portions are 22.72 units high. The domain for the run-up computations stretches from x=-461.17 to x=-29.35, which matches the length of the gas path from the injector face to the beginning of the test panel, and results in the boundary layer at the entry to the panel section having approximately the right characteristics. The domain for the panel computations stretches from x=-29.35 to x=121.15. The FFC injection manifold is modeled as a straight duct perpendicular to the panel wall, as seen below the x-axis in Figure 3, with a "height" which is five times its "length". This is a sufficient distance for a well-formed boundary layer to develop and to allow for the capture of the recirculation region within the duct.

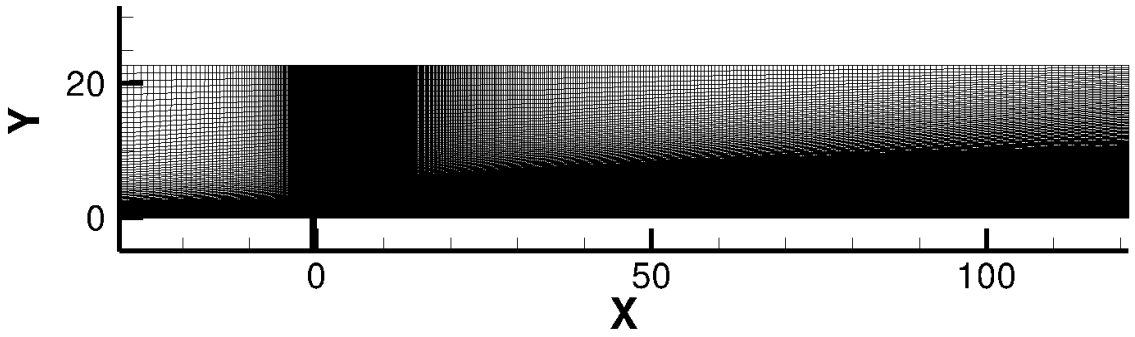

Figure 3. Mesh of 317,250 cells

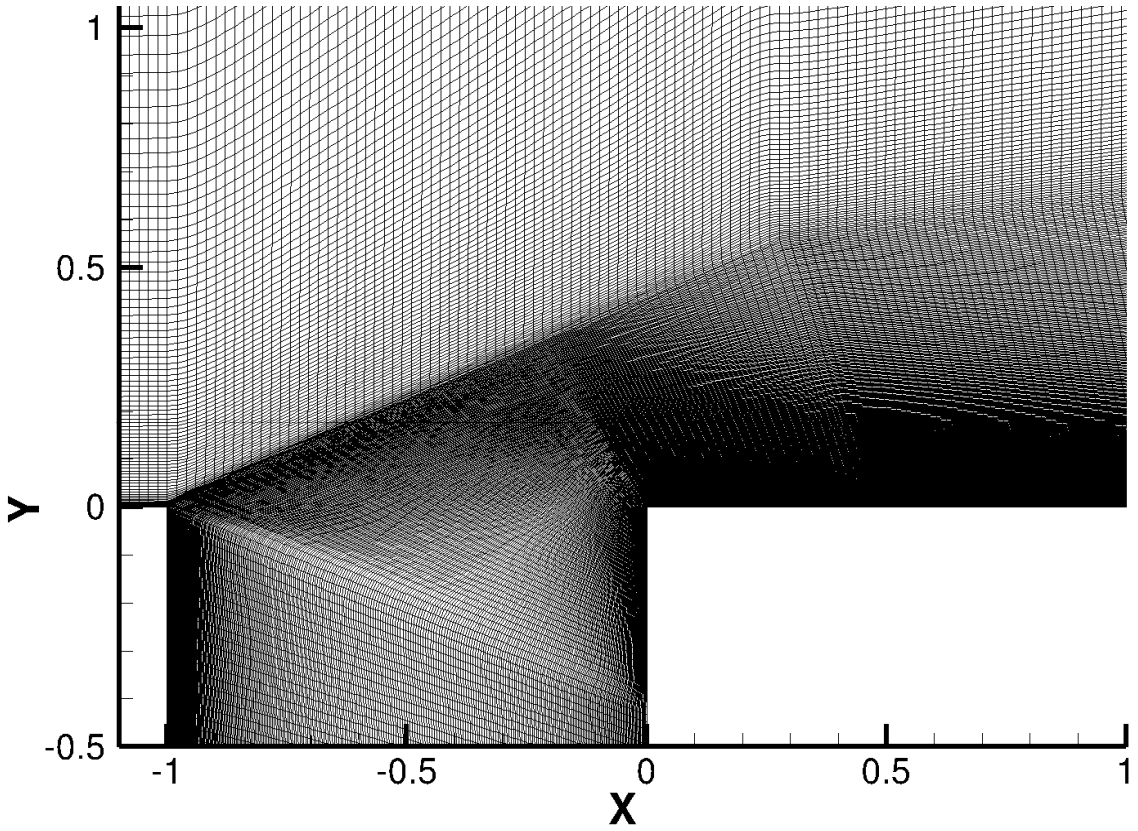

Figure 4. Close-up view of mesh near slot

The mesh used for all simulations involving the FFC panel and an injection slot is depicted in Figure 3. A close-up view near the slot is provided in Figure 4. This is a multi-block

structured mesh, with 11 blocks and a total of 317,250 quadrilateral cells. Its region of near-wall refinement extends further away from the wall than with typical boundary-layer meshes, in order to account for the thicker film. The mesh spacing distribution used to capture the shear layers was obtained iteratively by examining solutions on less optimal meshes. Near-wall mesh spacing was such that the wall-adjacent value of y+ lay between 0.5 and 1 for all the simulations presented here. This spacing should be sufficient for the k-ω turbulence model to resolve the momentum boundary layer satisfactorily. The mesh for the FFC panel without an injection slot is similar in resolution. The mesh for the run-up portion is also of similar resolution and has 114,000 cells.

We now list the boundary conditions and material property parameters specified for the simulations. For all simulations, symmetry conditions were specified at the artificial upper boundary and no-slip velocity conditions were specified at all walls. An exit pressure boundary condition with a uniform absolute pressure value of 717.7 psia was specified at the outlet for all simulations. Though the steady-state chamber pressure varied from run to run, these variations were neglected for the set of cases considered here, all of which were aimed at achieving a nominal chamber pressure of 700 psi. For all simulations, unless specifically indicated otherwise in the results section, a constant temperature condition with a temperature value of 800K was used as the thermal boundary condition at the wall surface at the lower boundary. As mentioned earlier, the need for this thermal boundary condition will be removed in the final full paper by employing conjugate heat transfer.

For the simulations of the run-up portion, the mass flow rate equal to the corresponding experimental setting is specified at the inlet, with the velocity assumed to be normal to the inlet and the velocity profile assumed uniform across the inlet. Wall boundary layers develop over the length of the run-up. The inlet temperature profile for all cases was set as a constant value of 3680 K, obtained as the adiabatic flame temperature from a CEA [4] calculation of the baseline case. Turbulence at the inlet was specified as a default turbulent intensity of 10% of the dynamic pressure. The simulations are relatively insensitive to the inlet turbulence level, and the turbulence adjusts to reflect the local flow conditions a short distance downstream of the inlet.

For the simulations of the panel portion, the inlet profiles of velocity, temperature, turbulent kinetic energy and turbulent specific dissipation were taken to be the run-up outlet profiles of the corresponding quantities obtained from the appropriate run-up simulation. The mass flow rates of the FFC flows were set to the corresponding values from the experiments, and the FFC inlet temperature was set to be 305 K for all cases. The mixture fraction variance was taken to be zero at both fuel and oxidizer inlets.

For both the run-up and the panel section simulations, the conserved mixture-fraction formulation in the non-premixed combustion model requires specification of fuel and oxidizer compositions, in order to build the PDF look-up table. The fuel was specified as kerosene vapor, and the 'oxidizer' composition was specified from an equilibrium computation performed of the primary flow of the baseline case using CEA [3]. The 'oxidizer' composition used is given in terms of mass fraction as [h2]=0.0061, [o2]=0.04414, [oh]=0.05646, [co]=0.35386, [o]=0.0132, [h]=0.00142, [h2o]=0.23882 and [co2]=0.286 (the species are indicated by the chemical formula used to identify them in Fluent). The limit on number of species to consider when building the table was set to be 12. This resulted in the consideration of the additional species methane and two forms of carbon among the product species. Trials with larger limits showed that further species are present with mass fractions of 10^{-7} or less. The molecular thermal conductivity of the multi-component fluid formed by any mixture of the 12 species was set to be 0.07383 W/m-K and its molecular coefficient of viscosity to be 3.7903×10^{-5} Pa-s. These are the values of the properties of the hot combustion products at 800K, as estimated using CEA [3]. The optical properties of the fluid mixture were set as follows: absorption coefficient = 100 per meter, scattering coefficient = 0, refractive index = 1.

The numerical scheme selected in Fluent to solve the model used second-order spatial finite-volume discretization. The CFD solver mode used to obtain the steady-state solution for all cases was the pseudo-transient relaxation method for the coupled pressure-based scheme, with automatic time step selection and a time-scale factor of 0.01. The solution was considered converged when the residuals dropped by five to eight orders of magnitude.

PRELIMINARY RESULTS AND DISCUSSION

We present, in this extended abstract, results from the preliminary simulations performed with the model limitations as described. Most of the model limitations, with the exception of accurate soot and coking modeling, are currently being addressed with improvements in the model, which is being tested and is expected to provide improved predictive capability in the final and full version of the paper.

All cases presented here have nominal conditions of a 700 psi chamber pressure and a mixture ratio of 2.8. The case with large CMFR and FFC=1.5% is regarded as a baseline case.

Figures 5 through 12 are flooded contour plots of field variables characterizing the numerical solution of the baseline case. Contour plots for the other simulation cases are not shown because they exhibit similar features.

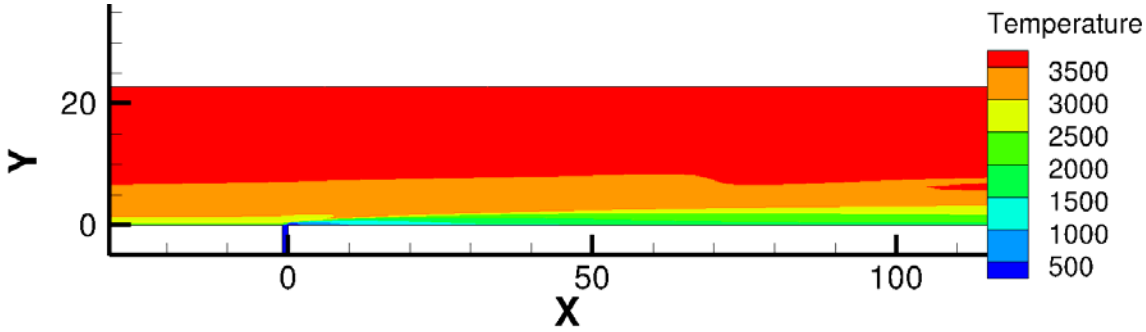

Figure 5. Contours of temperature (K)

The temperature field in the entire computational domain is shown in Figure 5. In the vicinity of the lower boundary representing the chamber wall, we see the cooling effect produced by the injection of cool fuel at x=0 and its subsequent transport to the outlet downstream as a layer adjoining the wall. Note that temperatures in the film rise as the film fluid moves downstream, as a result of mass and heat exchange with the hot core flow. Note also that temperatures at points close to the wall and equidistant from it are lower at x=120 than at x=20. However, the temperature drop from the core flow to 2500 K happens across a smaller distance at x=120 than at x=20.

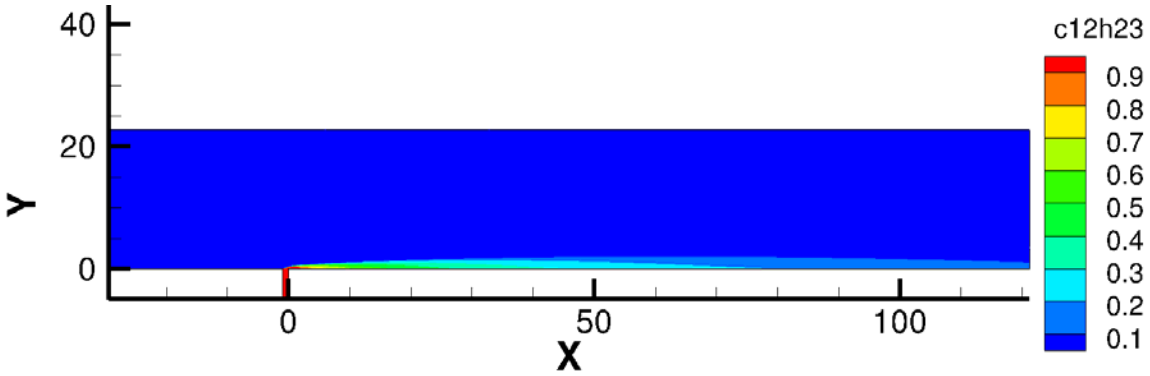

Figure 6. Contours of mass fraction of kerosene

From the contours of the mass fraction of kerosene (the simulant for RP-2 used in these computations) in Figure 6, we see that due to turbulent mass and heat exchange with the core flow, the equilibrium composition of the fluid in the film changes as it proceeds downstream. When the film fluid reaches x=60, the mass fraction of kerosene is less than 40%, and when it reaches the outlet, the mass fraction is less than 20%. This is caused mostly by change in the

chemical composition as the film heats up, and to a lesser extent by turbulent mass diffusion of the kerosene in a direction away from the wall. This is also seen in contours of the mean molecular weight of the mixture (not shown here).

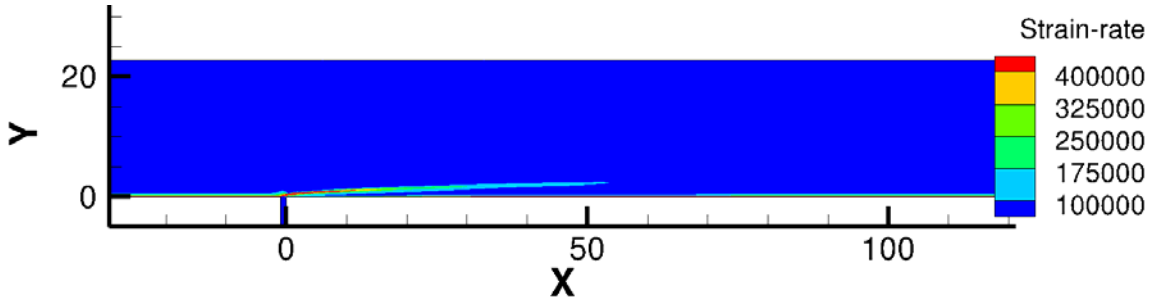

Figure 7. Contours of strain-rate magnitude (s^{-1})

Contours of the strain-rate magnitude in Figure 7 show the presence of a shear layer between the fast-moving core flow and the slower wall film. The strain-rate values in units of "per second" show high levels of shear in the layer, which will significantly affect the turbulence in the film, though even higher shear exists between film and wall at the wall surface.

Figures 8 through 12 are contour plots viewed from close-up near the slot.

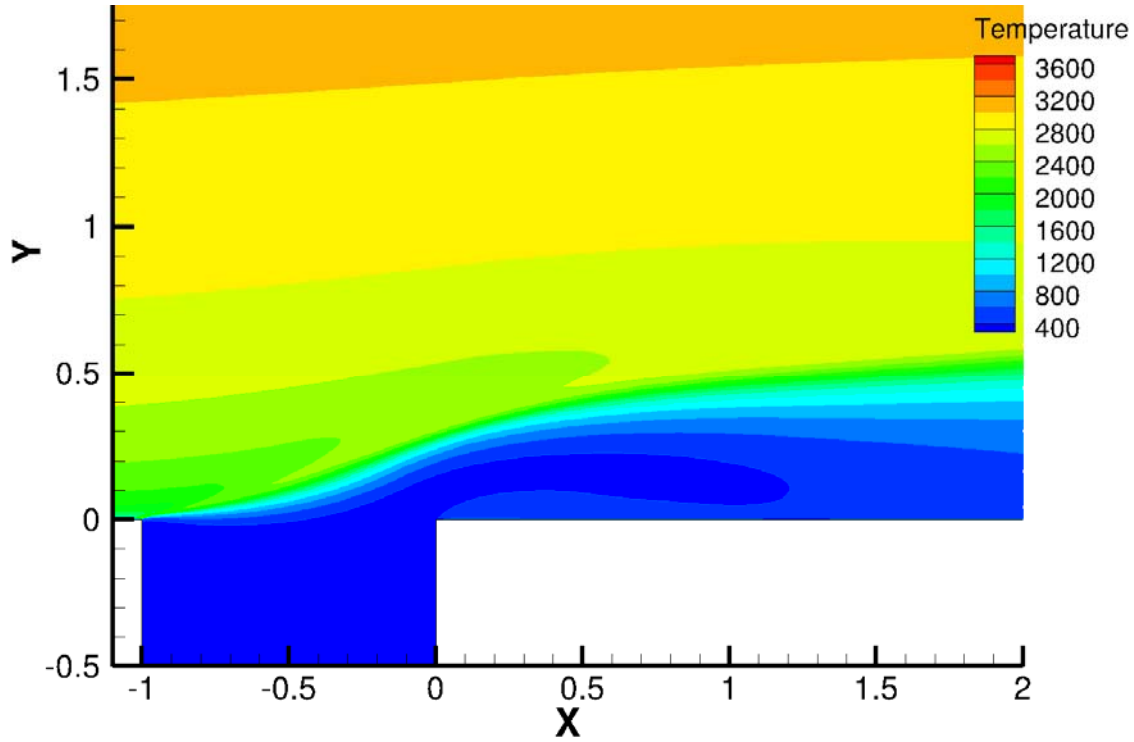

Figure 8. Contours of temperature (K) near slot

Temperature contours in Figure 8 show that the injected fuel jet does not penetrate very far from the wall, but is rapidly turned and forced to travel adjacent to the wall by the much larger momentum flux of the core flow. There is a wall-adjacent region immediately downstream of the trailing lip of the slot where the fluid temperature lies between 600 K and 800 K, which is higher than that of the injected fuel. This is clearly caused by the error in assuming the wall surface there to be at 800 K, which results in heat transfer from the wall to the fluid rather than the other way around. This error can be avoided by either the collection of experimental wall temperature

data or the inclusion of conjugate heat transfer in the simulation; the latter approach is planned for the improved model to be presented in the final paper.

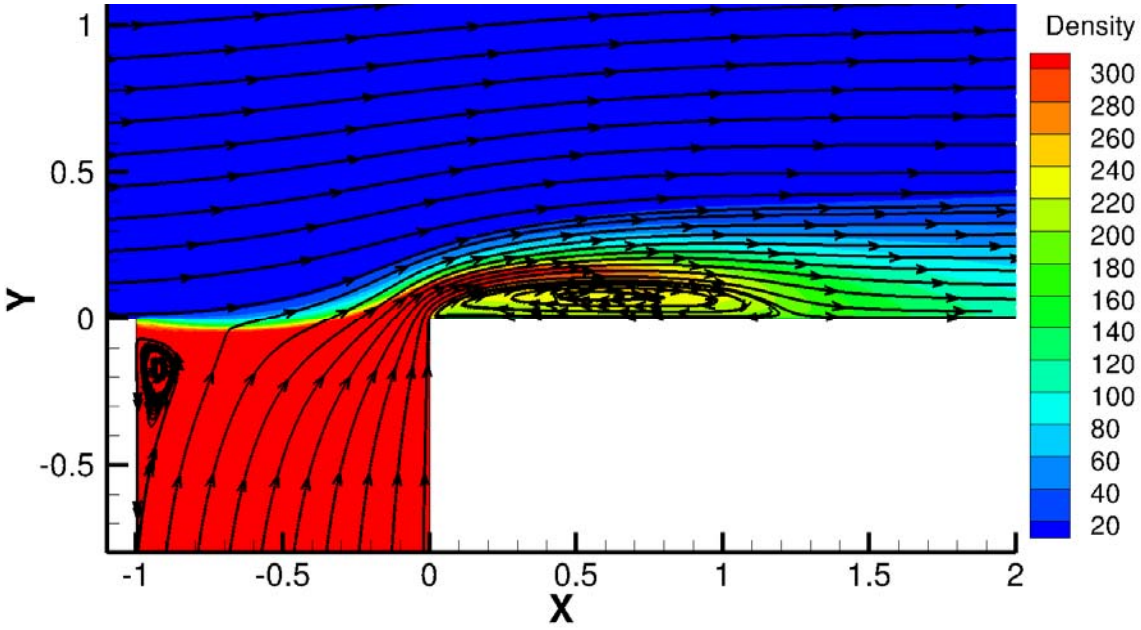

Figure 9. Contours of density (kg/m^3) near slot, with streamlines

Density contours in Figure 9 show the error inherent in the ideal gas equation of state implicit in using the kerosene vapor from the Fluent fluid materials database as a simulant for RP-2. The density of the fuel before it enters the chamber is seen to be only about a third of what is expected for 'liquid' kerosene at that high pressure. However, the mass flow rate and temperature of the injected fuel, which are the main factors in its initial cooling effect, match the conditions of the experiment. The error in density causes an error in the injection velocity, but the cooling effect of the film is insensitive to this at such high momentum flux ratios between core flow and injected fuel. Contours of other thermodynamic properties such as specific heat (not shown here) show similarly large variations across the domain. The overlaid streamlines show two recirculation regions, one within the injection manifold on the left wall and a larger one immediately downstream of the trailing edge of the slot. The second one may play a role in explaining counter-intuitive experimental heat-flux data in that region. It will also have a role in determining the level and distribution of turbulent kinetic energy within the wall film. The sizes of these recirculation regions vary, depending on the FFC mass flow rate. Even without considering chemistry or heat transfer, the fluid mechanics of a jet issuing into a cross-flow and mixing with it is quite a complex topic, though it has not been the focus of this study.

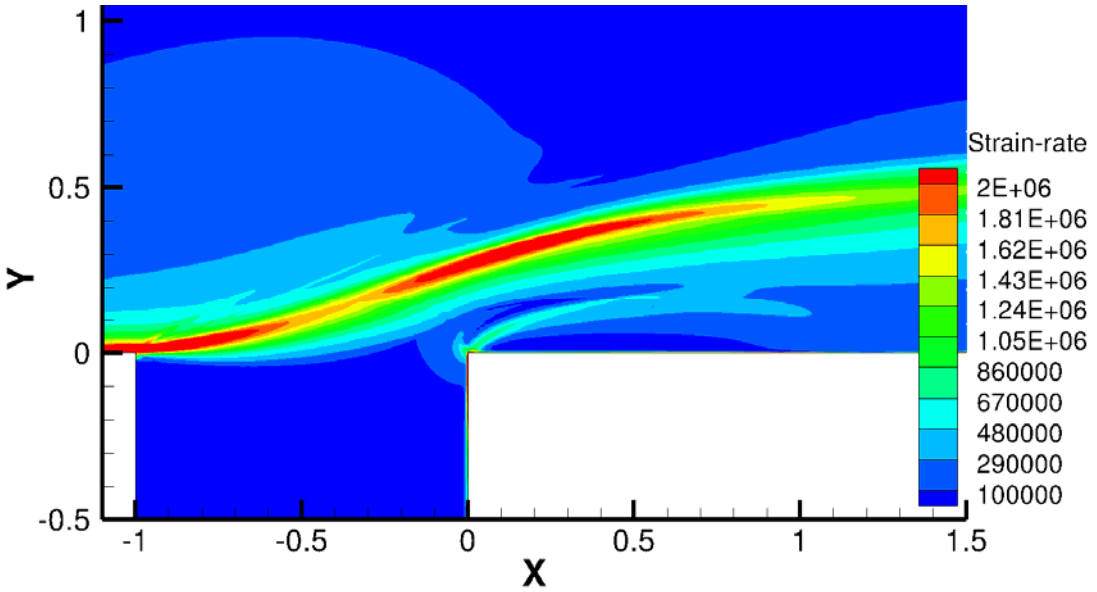

Figure 10. Contours of strain-rate magnitude (s^{-1}) near slot

The close-up of the strain-rate magnitude contours in Figure 10 shows not only the shear layer that demarcates the film from the core flow, but also a shear layer between the film and the recirculation bubble. The shear layers are regions of high strain-rate magnitude.

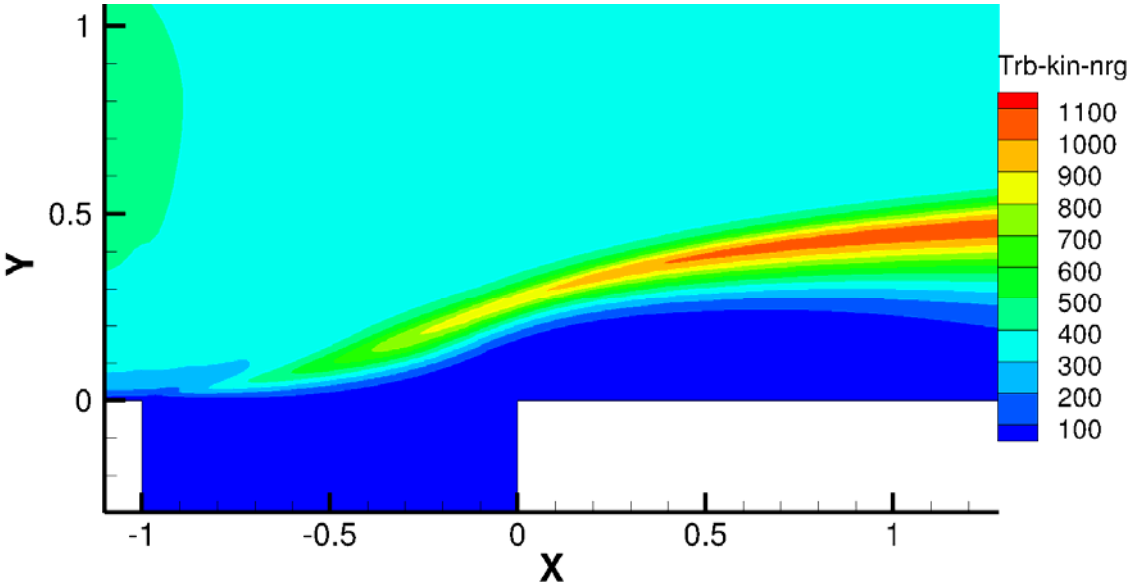

Figure 11. Contours of turbulent kinetic energy (m^2/s^2) near slot

Figure 11 shows that turbulent kinetic energy is created in the shear layer between core flow and film and is convected downstream.

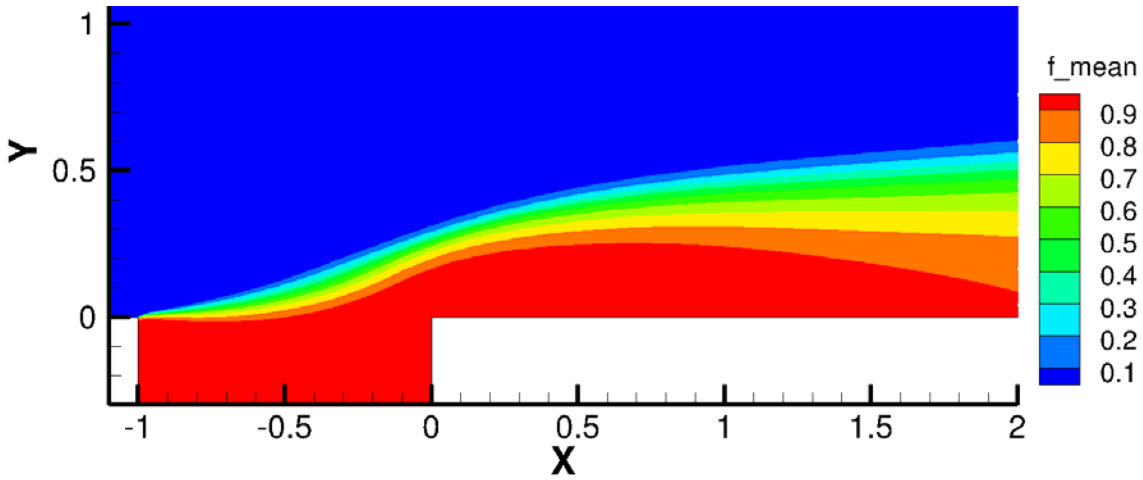

Figure 12. Contours of mean mixture fraction near slot

The contours of mean mixture fraction in Figure 12 are consistent with the temperature and density contours in Figures 8 and 9. The fuel is emerging from the slot, being forced to flow along the wall and transforming chemically into products of the equivalent of pyrolysis within the current model. Contours of the mass fraction of kerosene (not shown here) reflect the mean mixture fraction contours. However, examination of the mass fraction of other major species in the mixture (also not shown here) shows that the composition transformations are spread across an appreciably thick layer between core flow and wall. This is the equivalent of a "reaction zone" within the current equilibrium chemistry model, and it is found to be not sharp but relatively thick.

Figures 13 through 22 are line plots comparing results of various simulations with each other and in some instances with experimental data. All heat fluxes have been normalized with the value of the wall surface heat flux at the entry of the core flow into the test section as predicted by the simulation for the large CMFR cases.

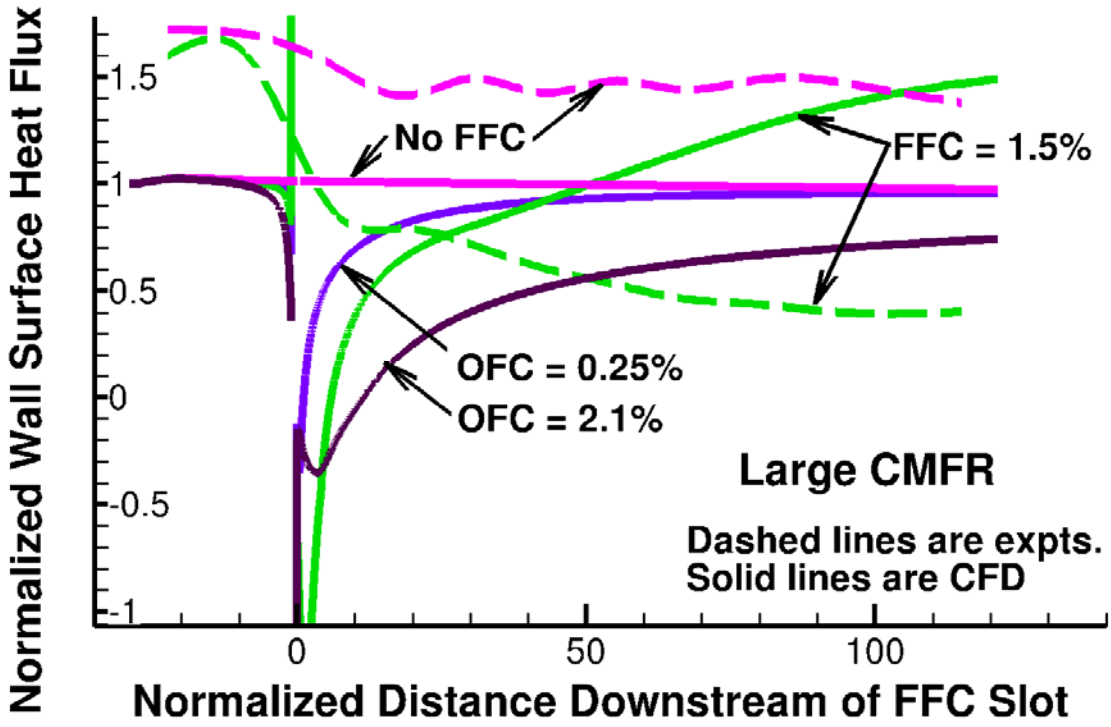

Figure 13. Wall surface heat flux profiles along wall

The experimentally observable wall surface heat flux, taken as positive when heat is transferred from fluid to wall, is plotted against normalized distance downstream of the slot in Figure 13 for several cases with the large CMFR. The solid curves are CFD simulation results, while the dashed lines are experimental data. We see in the case when no FFC was present, shown in purple, that both CFD and experiment show a basically horizontal shape, though the CFD value is only about two-thirds of the experimental value when radiation is not included in the CFD model. This relatively constant behavior is to be expected, because the thermal boundary layer and the driving temperature difference are not changing very much.

Turning now to the case of nominal FFC mass flow rate of 1.5%, shown in green, the story is very different. Upstream of the slot, the CFD matches the CFD of the no-FFC case. We must discount the CFD result immediately downstream of the slot, as it shows negative heat transfer, i.e. heat being transferred from wall to fluid. This is of course an outcome of the applied thermal wall boundary condition of 800K temperature, which creates a large error there because the adjacent fluid is relatively cool. The experimental data (green dashed line) show a large film cooling effect downstream of the slot. However, one puzzling aspect of the experimental data is that the heat flux at the first calorimeter downstream of the slot is not lower. It might be expected that the cool fuel issuing from the slot has not traveled far enough downstream to be heated enough by turbulent convection from the hot gas to produce the observed heat flux. Another puzzling aspect of the experimental data is that the film cooling effect increases with distance from the slot for about the first two-thirds of the cooled panel, i.e. the heat flux decreases. This increasing cooling may be due to increasing thickness of the layer of coke that is created on the wall surface, which acts as a thermal barrier. The CFD shows a quite contrary tendency, with the heat flux increasing as one goes downstream, reflecting the heating of the film by the core flow. The heat flux further than x=60 actually exceeds the value for the CFD case without the FFC, eventually considerably exceeding it.

We attempted to understand whether the heat flux was being increased beyond the no-FFC levels by chemical heat release effects. In the current model, as implemented in the non-premixed combustion formulation in Fluent, it was not possible to inject the kerosene and not have it reach chemical equilibrium with the “oxidizer” comprised of the hot combustion products. We did the next best thing, which was to replace the injected fuel with the “oxidizer”. This results in the mean mixture fraction being zero throughout the domain, indicating virtually no change in chemical composition. Two cases were run with two different oxidizer injection rates. These are OFC=0.25% and OFC=2.1%, and are marked correspondingly in Figure 13, where ‘OFC’ stands for ‘Oxidizer Film Cooling’. The lesser flow rate was an attempt to match volume flow rate with FFC=1.5% and the greater flow rate was an attempt to match thermal cooling capacity rate based on sensible enthalpy with FFC=1.5%. These curves behave more in line with intuitive expectations, with both the films showing a cooling effect, the greater flow rate showing a greater cooling effect, and both of them asymptoting towards the no-FFC heat flux as each film heats up. There appears little likelihood of either case exceeding the no-FFC heat flux further downstream.

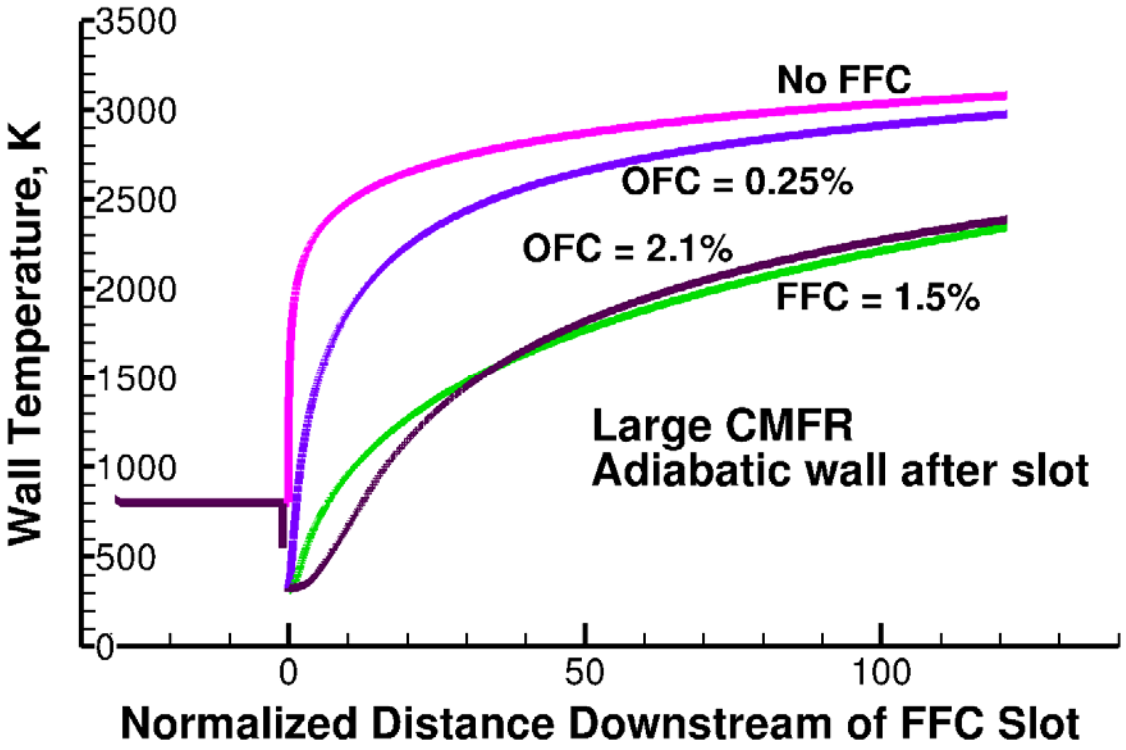

Figure 14. Profiles of adiabatic wall temperature along wall

In Figure 14, we present results of further cases that were run to try to understand the seeming inconsistencies among the CFD results. The same four cases were run as in Figure 13, with the difference that the thermal wall boundary condition downstream of the FFC slot was changed to a zero heat flux or adiabatic wall condition. The plotted wall temperature is then the so-called 'adiabatic wall temperature'. In the textbook of Kays et al. ([6], Eq. 16-24 and accompanying discussion), it is shown for some model cases that the surface heat flux can be written as the product of an effective thermal conductance and the difference between adiabatic and actual surface wall temperatures. This representation is stated to have broader applicability than proved there. The concept can also be found in other books and papers. The adiabatic wall temperature is here the high temperature in the temperature difference that drives the heat transfer. From the figure, we see that that in the no-FFC case the adiabatic wall temperature rises downstream of the slot as the boundary layer that was cooled upstream of the slot gets heated by the core flow. We see that the small oxidizer injection rate produces some cooling potential relative to the no-FFC case and that the large OFC produces a larger cooling potential. Matching intuitive expectations, the FFC=1.5% fuel injection is seen to produce approximately the same cooling potential as the larger OFC case. The chemistry seems to have little effect on the cooling potential.

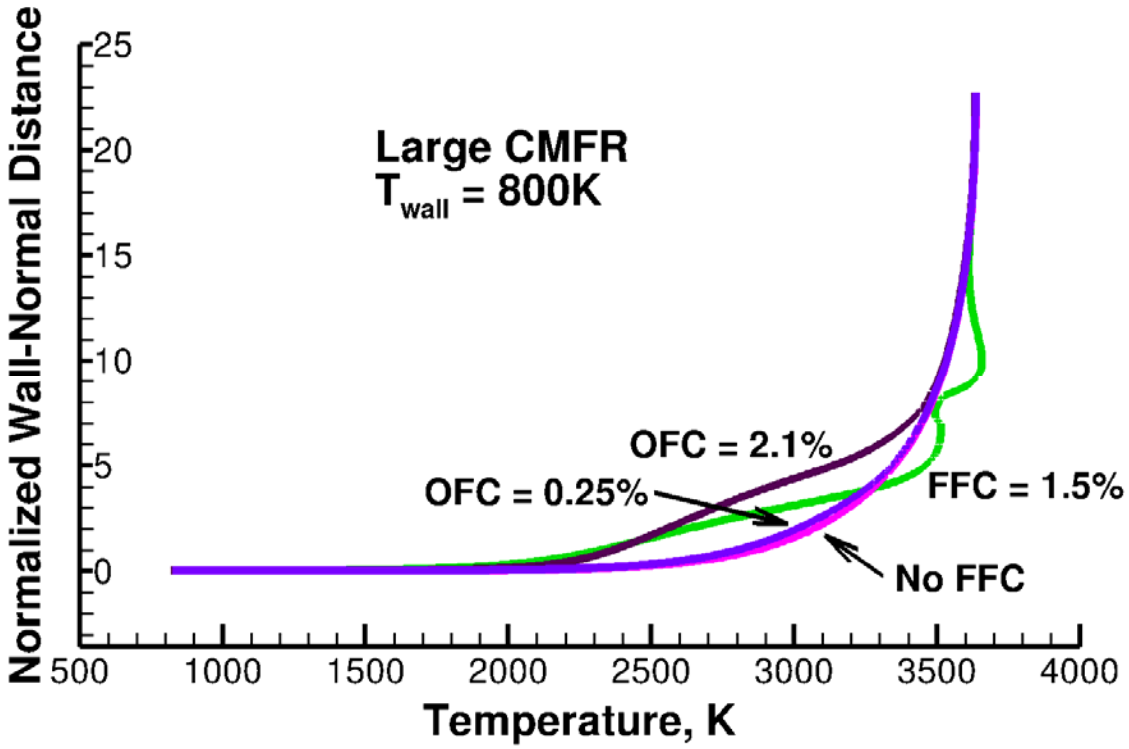

Figure 15. Profiles of temperature at the outlet, at x=121.15

Examination in Figure 15 of temperature profiles at the domain outlet in the same CFD cases as discussed in Figure 13 reveals that the temperatures for the FFC=1.5% and OFC=2.1% cases deviate quite substantially from the no-FFC case, in the film region away from the wall. The FFC=1.5% case even exhibits something that resembles a dual thermal layer. A close-up examination in the vicinity of the wall (not shown here) reveals that the normal gradient of temperature for all cases is almost the same. The resolution of the paradox posed by Figures 13 through 15 must lie in the effective thermal conductance of the film.

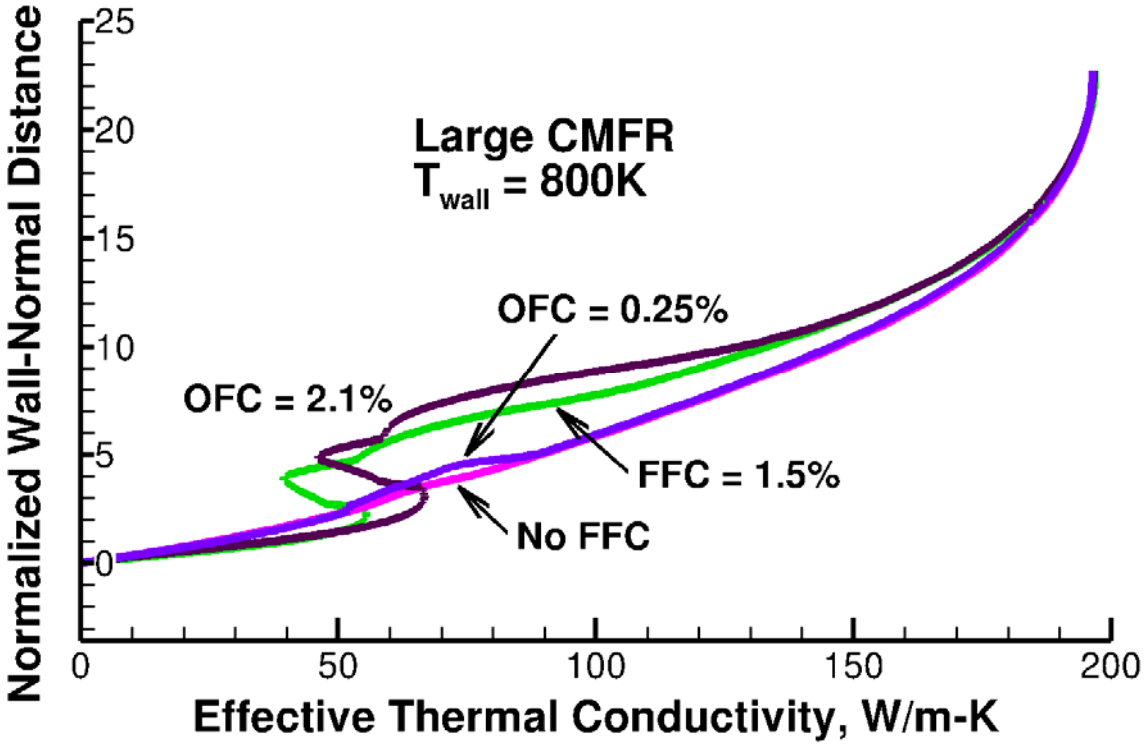

Figure 16. Profiles of effective thermal conductivity at the outlet, at x=121.15

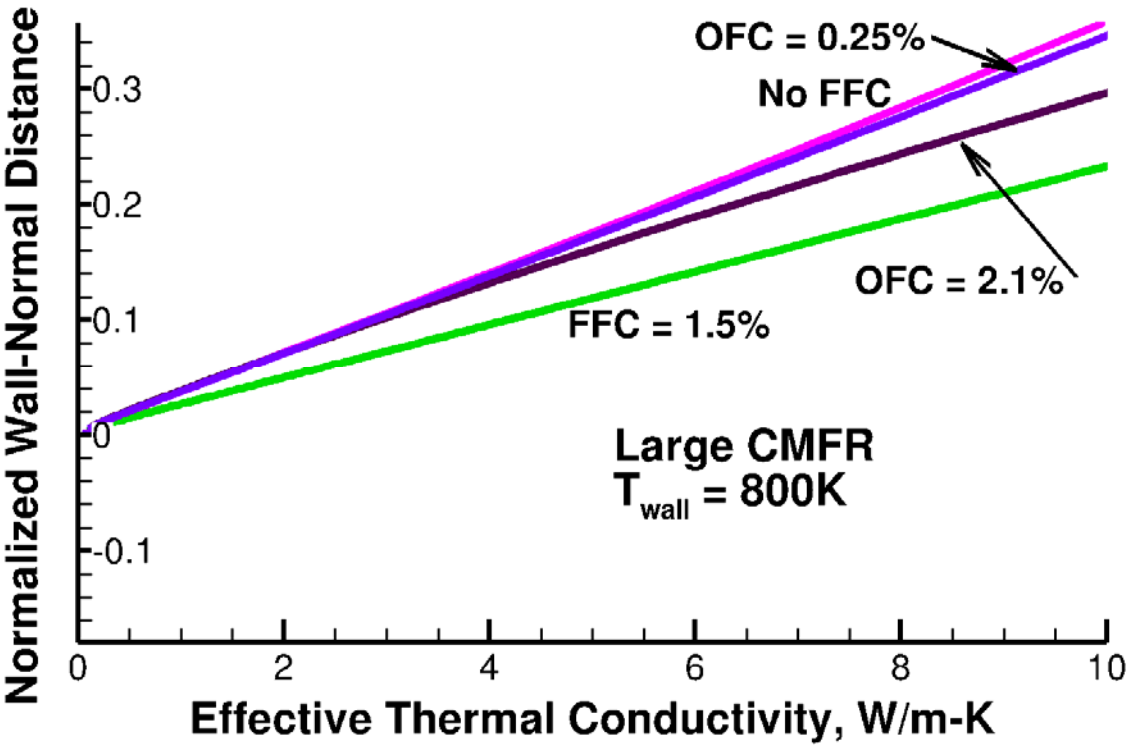

Figure 17. Close-up near wall of profiles of effective thermal conductivity at the outlet, at x=121.15

Figures 16 and 17 are plots of the effective thermal conductivity profiles at the domain outlet, for the same four cases as in Figures 13 and 15. The effective thermal conductivity is the sum of the molecular and eddy (turbulent) thermal conductivities. We see in Figure 16 that there is a local peak in the conductivity within the film for the FFC and larger OFC cases. This is likely due to the turbulence associated with the shear layer between core flow and film, and leads to the temperature distributions of Figure 15. Furthermore, in Figure 17 we see that all conductivities tend at the wall to the small but non-zero molecular thermal conductivity value that was prescribed to be the same constant value for all cases. The effect of turbulence diminishes to zero on approaching the wall. However, very near the wall, the conductivity in the FFC=1.5% case rises more rapidly with distance from the wall than for the other cases. This is likely to be related to the very different thermodynamic properties, such as the density and specific heat, of the film in the FFC=1.5% case as compared with the OFC=2.1% case. Furthermore, the wall heat transfer also depends on the thermal resistance of the laminar sub-layer of the boundary layer. . While the dependence of density and specific heat on both temperature and composition is correctly accounted for, the molecular thermal conductivity and molecular viscosity of the mixture are taken to be constant. Their dependence on the temperature, and particularly on the mixture composition, is neglected. This approximation may introduce a significant error in the computed wall heat transfer for the fuel-film-cooled cases, and explain the previously described anomaly. A test, not reported here, showed that the wall heat flux is quite sensitive to the molecular thermal conductivity value, an approximate doubling of the conductivity producing a 25% increase in the wall heat flux. Further understanding is needed of the calculation of wall heat transfer in Fluent, and of the effect on the wall heat transfer of composition-dependence of molecular and eddy thermal conductivity as well as molecular viscosity. In the final version of the conference paper, these aspects will be studied, and better modeling of the molecular transport properties will be used. This improvement of the model, which is currently being implemented and tested, is expected to eliminate the anomalous behavior described above. The results in the final full version of the paper are expected to underline the big contribution of the laminar sub-layer to the thermal resistance of the film and boundary layer, and to highlight the importance of accounting for the dependence of molecular transport properties on not only temperature but also mixture composition.

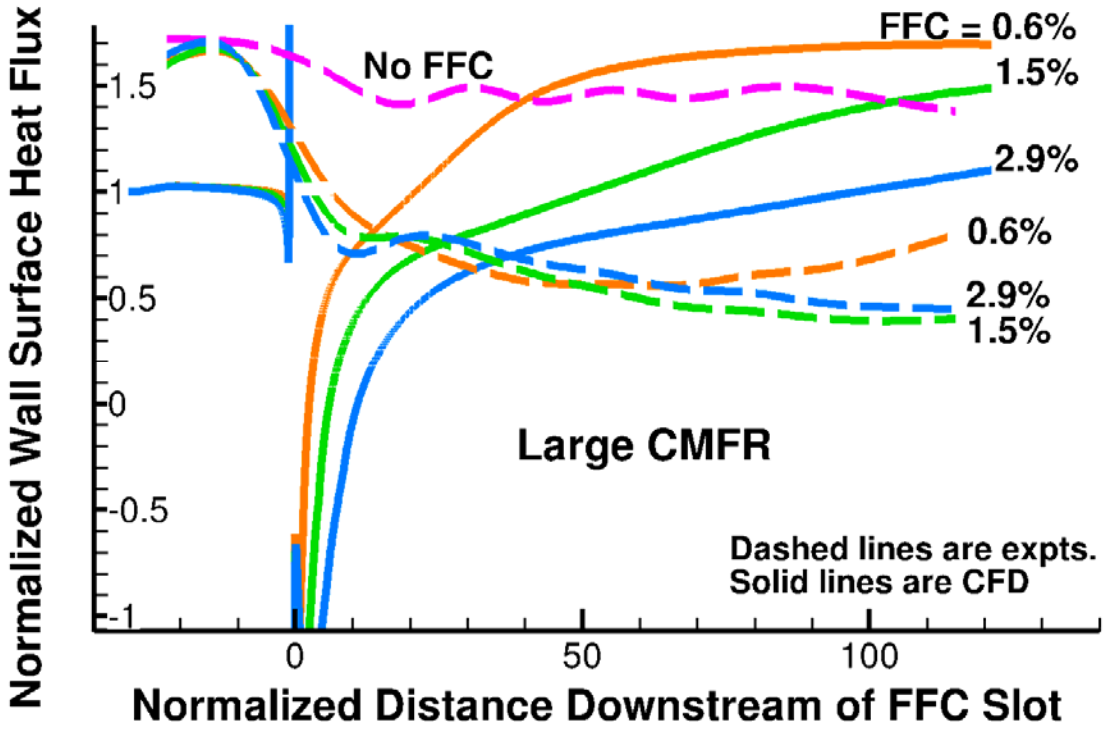

Figure 18. Comparison of CFD with Experiment for large CMFR and three FFC flow rates

Figure 18 shows the CFD predictions of wall surface heat flux for multiple FFC flow rates, all with the large CMFR, compared with the experimental data for the corresponding cases. At the first calorimeter downstream of the slot, the experimental heat flux shows the expected dependence on FFC flow rate, based on consideration of the sensible enthalpy. At the third through fifth downstream calorimeters, however, the experimental case with FFC=0.6% provides the most cooling, while further downstream it once more provides the least. From the third calorimeter onwards, FFC=2.9% provides less cooling than FFC=1.5%. Possibly, this experimentally observed behavior is due to the FFC=0.6% film heating up early and using up most of its soot capacity, while the FFC=2.9% stays cooler than the outer layer of the FFC=1.5% film and thus forms less soot. Clearly, the experimental data do not follow the classical scaling of a non-sooting non-reacting film. The simulation results in Figure 18 show the same trend as encountered in Figure 13, for all the FFC flow rates. The cooling predicted by CFD simulations scales positively with FFC flow rates in a manner consistent with the physics included in the model.

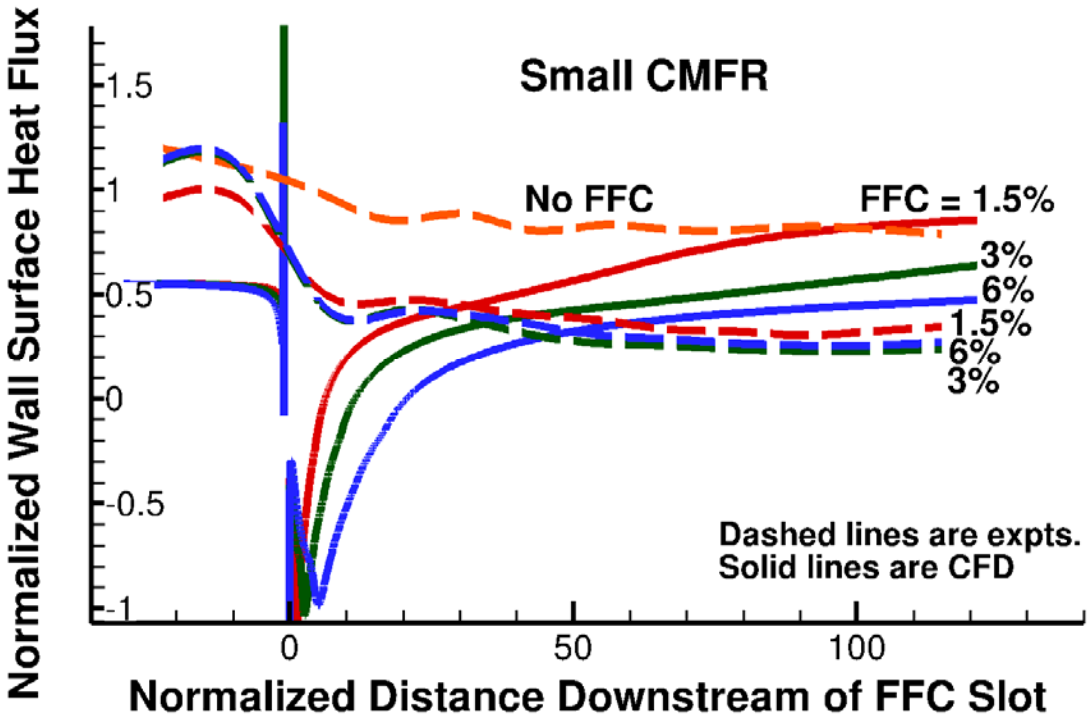

Figure 19. Comparison of CFD with Experiment for small CMFR and three FFC flow rates

In Figure 19, we see much the same trends in the simulation results for multiple FFC flow rates with the small CMFR, as compared with experimental data.

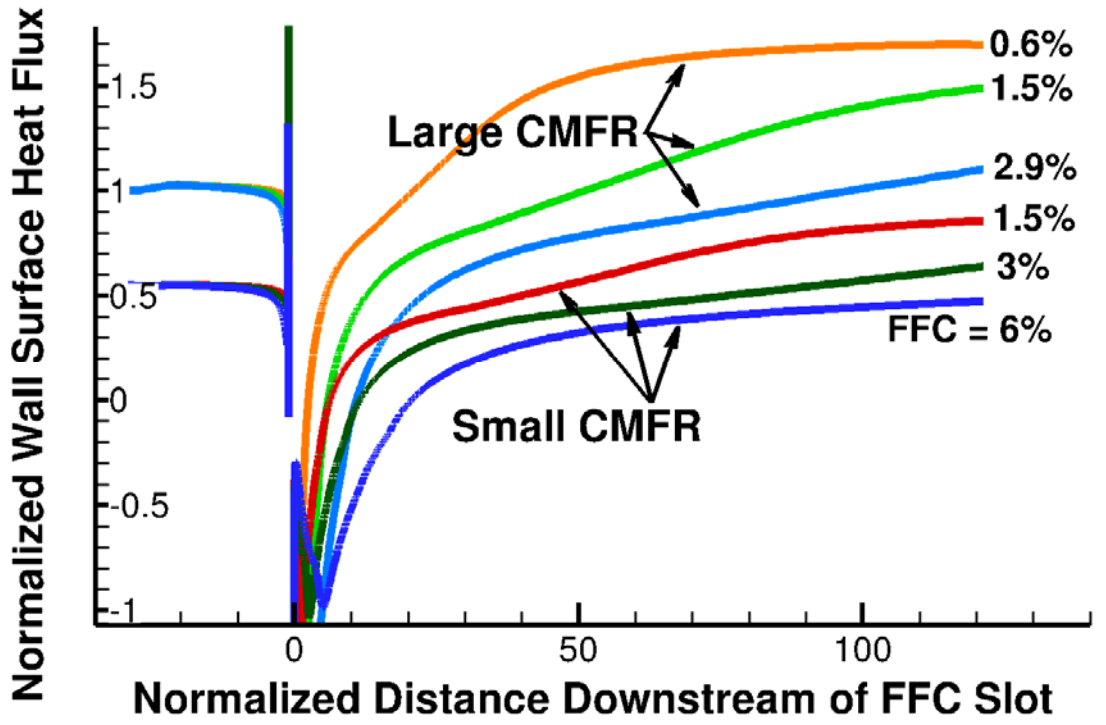

Figure 20. Sensitivity of Wall Heat Flux to CMFR and FFC flow rate

The simulation results of the previous two figures are re-plotted in Figure 20, for convenient comparison with each other. The large CMFR cases have a larger core gas speed than the small CMFR cases. It is seen from the figure that the model shows the expected increase in convective heat flux with increase in core gas speed.

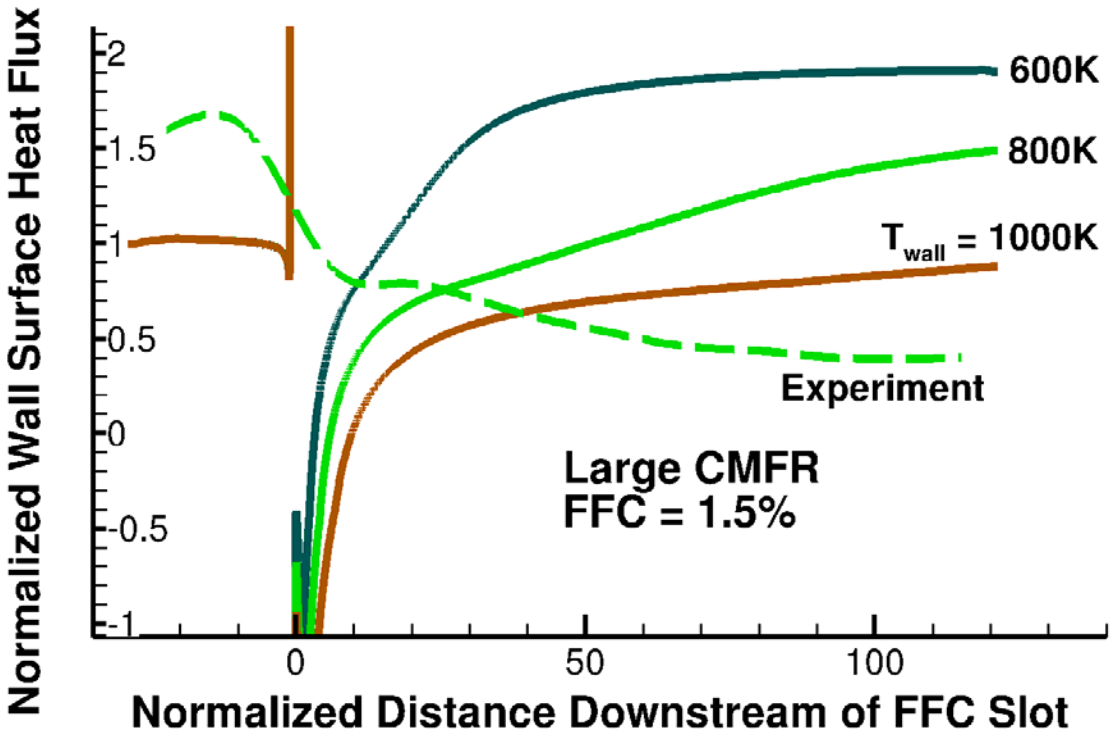

Figure 21. Sensitivity of Wall Heat Flux to Assumed Wall Temperature

We examined the sensitivity of the predicted heat flux to the assumed value of constant wall temperature, and the results are shown in Figure 21 for the baseline case. The wall temperature upstream of the slot was always set to 800 K, but the temperature downstream of the slot was set to the values listed for the three curves. The predicted heat flux is seen to be significantly influenced by the wall temperature, and changes with the latter in the expected direction. This underlines importance of either specifying realistic values of wall temperature, perhaps from planned experiments, or else performing a conjugate heat transfer analysis, as planned for the final full paper, which would remove the need to specify the wall temperature. A wall temperature of 1000 K is seen bring the CFD prediction closer to experiment, but this is not a realistic temperature.

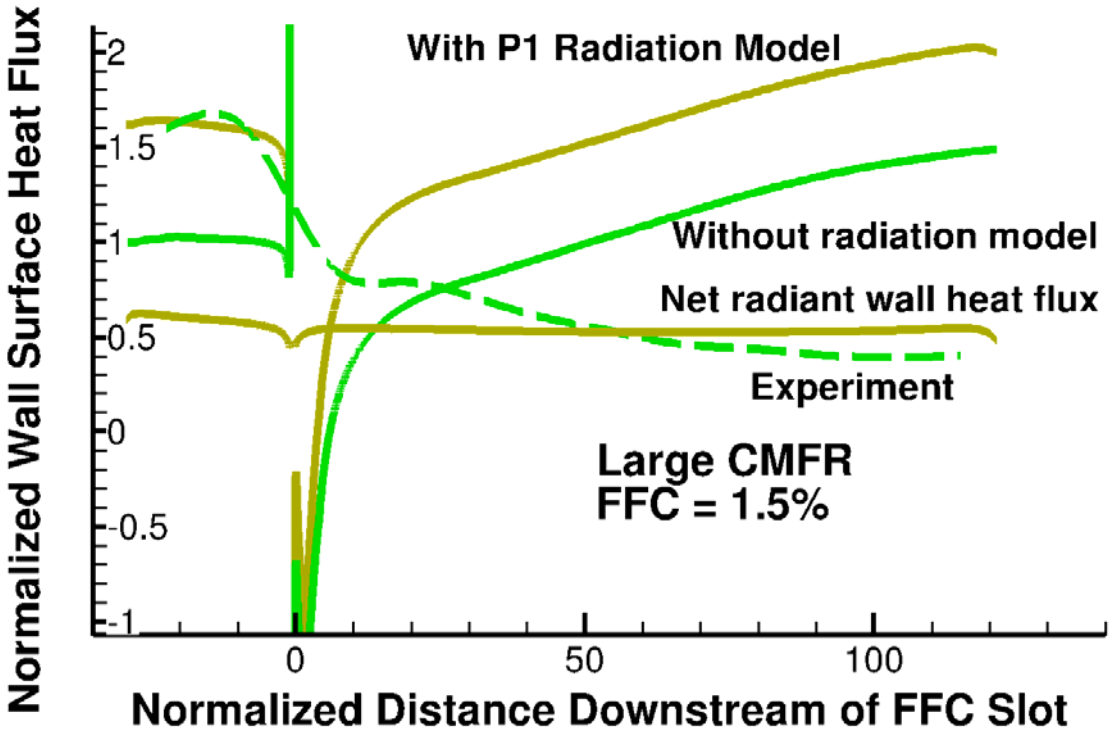

Figure 22. Estimate of Radiative Heat Transfer Effect on Wall Heat Flux

Finally, we examined the sensitivity of the heat flux to radiative heat transfer. For the baseline case, we included the P1 model available in Fluent. This augments the CFD model by solving the radiative transfer equation in a participating medium. We assumed that the fluid mixture is a gray medium, wherein the absorption coefficient is independent of the wavelength of the radiation. An absorption coefficient of 100 per meter was used. The wall temperature was maintained at 800 K, and the wall was treated as a black body radiator. The results are shown in Figure 22. We see that the predicted radiant wall heat flux is of a magnitude comparable to the predicted convective heat flux. Therefore, a key finding is that under the conditions of the laboratory experiments, thermal radiation plays a sizable role, and must be accounted for in the mathematical model. Remarkably, it is noticed that upstream of the FFC slot, the CFD prediction of heat flux with radiation included matches the experimental value fairly closely. Without further numerical experiments, it is not possible to rule out that this agreement is the outcome of a fortuitous choice of radiation absorption coefficient or wall temperature.

SUMMARY AND CONCLUSIONS

A model was constructed for the numerical simulation of heat transfer to walls that are cooled by injection of a cool fluid through a wall slot. The fluid physics model comprises a steady-state, compressible flow model with convective and radiative heat transfer, with a RANS turbulence model, and with equilibrium chemistry in a conserved mixture-fraction formulation. We attempted to validate the model with experimental wall heat-flux data, and preliminary simulations were performed, which are reported in this abstract. Simplifying approximations and omissions made while constructing the fluid model and the model of the experimental arrangement were listed and discussed. The preliminary results showed that the use of constant values of molecular transport properties as well as the use of a constant temperature wall boundary condition resulted in significant errors. These simplifying assumptions that significantly impaired the accuracy of the model will be addressed with an improved model currently being implemented and tested, and the improved model is expected to yield improved predictions which will be reported in the full version of the paper to be presented at the conference. The influence of carbon deposits on the wall thermal resistance will only be addressed by introducing a constant wall thermal resistance in the full paper. More sophisticated treatments will be deferred to future work.

The CFD simulations predicted flow fields and wall surface heat transfer that display trends expected from the physics model used in this study, for example trends with respect to changes in CR and FFC flow rate. An apparent inconsistency in the CFD predictions was investigated, namely that the wall heat flux far downstream of the FFC slot location was higher with a fuel film than without. Simulations revealed that the fuel film at the wall lowered the adiabatic wall temperature relative to the no-film case, consistent with expected physics. This inconsistency likely arises from not accounting for the composition-dependence and temperature-dependence of the mixture molecular transport properties in the laminar sub-layer, or from a higher near-wall turbulent conductivity caused by turbulence in the denser, higher-specific-heat fuel film. These matters will be studied in the final version of the conference paper, and an improved model with composition-dependent transport properties will be presented.

The wall heat flux predictions obtained from the current model are of the same order of magnitude as the experimental measurements. However, these preliminary predictions are not in full agreement with the values or trends of the experimental data. The exception was that good agreement was seen between CFD and experiment in a case with no FFC and which included radiative heat transfer in the CFD model. However, an improved version of the model is expected to result in improved wall heat flux predictions under non-coking conditions, and will be reported in the final version of the paper.

A key finding of the current study is that thermal radiative heat transfer is significant under the conditions of the experiment. It therefore must be included in the model in order to predict the level of heat flux found in the experimental data.

The current model is a first step towards reliable and accurate prediction of fuel film cooling effectiveness. However, it is missing some important physics, and consequently it does not provide insight into non-classical scaling behavior of the heat flux as observed in experiment. On the basis of experimental evidence, candidates for missing physics are soot formation/oxidation, wall coke build-up, non-equilibrium hydrocarbon pyrolysis/oxidation chemistry, proper thermal representation of the wall through realistic wall temperatures or conjugate heat transfer, and strongly temperature- and composition-dependent fluid properties, especially in the laminar wall sub-layer. In the final version of the paper, as previously mentioned, conjugate heat transfer will be used to eliminate the inaccurate wall temperature boundary condition. In the full paper, we also plan to study the sensitivity of heat transfer to molecular fluid property variations, and more accurate fluid mixture molecular transport properties will be employed. The paper will demonstrate the importance of accounting for the dependence of these properties on mixture composition, in order to get correct heat flux values. We also plan to study the sensitivity to mesh spacing y+ and the choice of RANS turbulence model. We expect that with the planned model improvements, the model should provide good estimates of both wall temperature and wall heat flux under non-coking conditions.

FUTURE WORK

The identified weaknesses of the current model provide the directions for future efforts to improve the model and use it to optimize the FFC technology. In further model improvements, thermal radiation must be an integral part of the model, with realistic estimates of mean absorptivity and emissivity of a soot-heavy dense fluid. The next step toward more accurate thermochemistry will be to include moderately non-equilibrium pyrolysis chemistry via a flamelet model. This may further allow the incorporation of soot formation and oxidation within the conserved-scalar/flamelet formulation. The model will then be extended to include coke deposition on wall and the associated thermal barrier effect. The sooting and coking may require a switch to the more expensive finite-rate chemistry formulation. Another topic of future study is the interaction between successive FFC slots and its impact on optimal slot placement.

REFERENCES

1. Yang, W. and Sun, B., ***Numerical Simulation of Liquid Film in a Liquid Oxygen/Rocket Propellant 1 Liquid Rocket***, Journal of Thermophysics and Heat Transfer, Vol. 26, No. 2 (April-June 2012).
2. Kirchberger, C., Schlieben, G. and Haidn, O.J., ***Assessment of Analytical Models for Film Cooling in a Hydrocarbon/ GOX Rocket Combustion Chamber***, AIAA 2012-3909, 48th AIAA/ASME/SAE/ASEE Joint Propulsion Conference & Exhibit, Atlanta, GA (July 2012).
3. McBride, B.J., ***CEA – Chemical Equilibrium with Applications***, at http://www.grc.nasa.gov/WWW/CEAWeb/ (accessed March 2013).
4. Modest, M.F., ***Radiative Heat Transfer***, Third Edition, Academic Press, Amsterdam, the Netherlands (February 2013).
5. Peters, N., ***Turbulent Combustion***, Cambridge University Press, Cambridge, U.K. (2000).
6. Kays, W., Crawford, M., Weigand, B., ***Convective Heat and Mass Transfer***, 4th ed., McGraw-Hill, New York, NY (2005).
7. Wang, T.-S., "Thermophysics Characterization of Kerosene Combustion," ***Journal of Thermophysics and Heat Transfer***, Vol. 15, No. 2, 2001, pp. 140–147.